JMEPEG (2021) 30:8276–8288
https://doi.org/10.1007/s11665-021-05997-6

1059-9495/$19.00

Effect of Particle Size and Morphology on Critical Velocity and Deformation Behavior in Cold Spraying

Lopamudra Palodhi, Biswajit Das, and Harpreet Singh

Submitted: 16 March 2021 / Revised: 21 May 2021 / Accepted: 14 June 2021 / Published online: 6 July 2021

Experimental investigations, coupled with numerical simulations, reported in the literature have documented the effect of particle size quite systematically. However, similar systematic studies on the role of particle morphology are lacking in the literature, although numerous experiments suggest a qualitative dependence of the coating process on the morphology. In this paper, we attempt to address the lacunae by comparing the deformation behavior and critical velocity by systematically varying the particle morphology and size. We have considered two different shapes, viz., spherical particles (where the size has been varied) and conical particles (where the morphology has been varied as a function of the apical angle, in addition to varying the size). Equi-volume comparison between the spherical particles and conical particles with different morphologies allow us to establish quantitative dependence of deformation characteristics and critical velocity on the particle morphology. We demonstrate that the vertices in conical shapes are regions of high stress concentration and deform preferentially; furthermore, the larger the apical angle the more closely does the deformation behavior of the conical particles resemble the sphere. Therefore, a knowledge of the distribution of particle size and morphology is expected to help tune and optimize the processing conditions.

Keywords cold spraying, critical velocity, finite element analysis, particle morphology

1. Introduction

Cold spray is an emerging thermal spraying technique for solid-state deposition of powders on a substrate at a relatively low temperature. This mitigates issues associated with oxidation of the feedstock or temperature-dependent phase transformation of the deposits. The primary adhesion mechanism during the cold spray process is dictated by the deformation characteristics of the powder particle as it is sprayed on the substrate. Several parameters, such as particle velocity, material properties, powder size and morphology, affect the deformation processes and deposition efficiency. We investigate the role of particle size and particle morphology on the critical velocity and the deformation behavior during a cold spray process.

In cold spraying, the powder particles are accelerated at a high speed of around 500-1200 m/s inside a converging diverging De-Laval nozzle. After impingement on the surface, both particle and substrate plastically deform and kinetic energy of the powder particles is dissipated. A threshold particle velocity is required for the plastic deformation and sufficient (proper) adhesion of the coating (Ref 1-3). This threshold velocity is termed as the critical velocity. The critical velocity is dependent on various factors, viz., material properties of the powder as well as substrate (Ref 3-6), and the temperature of the particle prior to impingement (Ref 7, 8). Particle sizes and morphology were also reported to influence the particle velocity (Ref 9, 10) and hence the deformation on impact. The critical velocity for several materials was investigated by measuring the deposition efficiency (Ref 11) and finite element (FE) modeling (Ref 1, 11-15) . A well-established method for determining critical velocity using numerical technique was put forward by Assadi et al. (Ref 1). This technique is based on the concept of jet formation during adiabatic shear instability (ASI). The critical velocity was experimentally found to be 500 m/s and 650 m/s for Cu powder on Cu substrate and 316L stainless steel powder on 316L stainless steel substrate, respectively, for a spherical particle with diameter 25 μm. They also found that critical velocity decreases sharply as the particle size increases up to 50 μm. However, the effect of particle size becomes relatively negligible beyond the particle size of 50 μm (Ref 8). A parametric expression was also proposed by Assadi et al. (Ref 6) for the estimation of critical velocity that utilizes a term to consider the effect of particle size. An in situ observation of the effect of the particle size on the critical velocity was presented by Hassani-Gangaraj et al. (Ref 2) for Al particles on Al substrate. They showed that the critical velocity shifts from 810 m/s for the particle size of 15 μm to 770 m/s for the particle size of 30 μm. A number of other investigators (Ref 4, 16-19) also confirmed the fact that particles of a larger size could be deposited to form a coating with a lower critical velocity than the smaller size particles of the same material. Numerical studies on the effect of particle size showed that while the critical velocity decreases with increasing particle size, the deformation characteristics remain qualitatively same (Ref 20). Similar trend was also observed for the deformation indices, i.e., the flattening ratio and the compression ratio. These indices were also found to be decreasing with an increase in size of the powder particle

Lopamudra Palodhi and **Harpreet Singh**, Department of Mechanical Engineering, Indian Institute of Technology Ropar, Rupnagar, Punjab 140001, India; and **Biswajit Das**, Department of Mechanical Engineering, K. K. Birla Goa campus, BITS Pilani, Pilani 403726, India. Contact e-mails: lopa.palodhi@iitrpr.ac.in and plopamudra@gmail.com.

(Ref 7). Experimental studies by King et al. (Ref 21) on the deformation behavior of copper and aluminum particles on a rigid ceramic substrate, however, contradicted the numerical studies and demonstrated a dependence of the deformation behavior on the particle size. A reduced flattening ratio was observed for smaller particle sizes.

In addition to size, powder particles are also characterized by their morphology. In cold spray, researchers tend to use spherical particles because they are easier to bond, however, irregular powders are also available. Therefore, it is important to understand the deformation characteristics for non-spherical powder particles also. While the role of morphology has not been systematically investigated, it is expected that the powder morphology will influence the deformation behavior. An irregular shape of the particle possesses sharp edges in their geometry. These sharp edges may act as localized stress-raisers resulting in enhanced localized plastic deformation. Furthermore, non-spherical particles have a higher surface area in contact with the propellant gas in comparison with the spherical particles. Therefore, they have a higher drag coefficient and experience higher decelerating forces due to air resistance prior to impinging on the surface. Therefore, one expects higher initial particle velocities will be required for such particles for deforming and adhering onto the substrate as opposed to spherical particles. A higher critical velocity was found for irregular shaped Cu particles as compared to the spherical particles (Ref 18). For spherical- and irregular-shaped Cu particle, the critical velocities were found to be of 425 and 550 m/s, respectively. It was observed that the influence of the particle morphology on critical velocity is more pronounced for the larger particles (Ref 22). Several reports are present in the literature with irregular-sized Ti powders and their coating characteristics (Ref 23-26). It was found that for particle sizes from 16 to 22 μm, porosity increases (Ref 23); however, for particle sizes ranging from 28 to 47 μm porosity decreases (Ref 24). It was also shown that as porosity level decreases, the coating microhardness increases irrespective of the morphology of the particles (Ref 26). The effect of particle morphology and size distribution on cold-sprayed pure Ti coatings was also investigated experimentally by Wong et al. (Ref 7). A comparison was made between spherical, sponge and irregular powders. Higher average impact velocities were recorded for the sponge and irregular powders. Deposition efficiency was found to be higher for sponge and irregular particles as compared to the spherical particles. For spherical particles, the porosity was lowest for the particles with largest size.

Most of the work with varying particle size and morphology have investigated the bonding process and the properties of various coatings. For example, King et al. (Ref 21) studied the coating properties of Cu on Al_2O_3 and Al on PZT. Jodoin et al. (Ref 22) analyzed Al on Al coating including the hardness of the aluminum powder. They found that the irregular particles do not form as dense coatings as spherical particles owing to the higher hardness of the irregular particles. This work, however, only shows the difference of hardness of powders and no specific comparison have been made using different particle sizes. The work by Wang et al. (Ref 7) highlighted primarily the properties of cold-sprayed coatings, i.e., microhardness and porosity of pure Ti coatings for different particle morphology (Ref 11). They assumed that the relation is same for both spherical and irregular particles, which may or may not be true. No direct comparison was provided in the paper between the critical velocities obtained from the relation and experiments. Furthermore, the comparison between different particle morphologies was done for dissimilar particle sizes (the spherical particle diameter was 20-36 μm, sponge particle size and irregular particle size were 49 and 26 μm, respectively), as a consequence of which it becomes difficult to separate out the effects of particle size and morphology. Therefore, it is difficult to visualize a systematic comparison of the critical velocities as well as the deformation behavior. Defining the particle size using diameter is problematic for the irregular particles. We have used volume instead to define the size of both spherical and irregular particles, which is more consistent and hence a direct comparison is adopted for the particles with different morphology. For a given volume and density, the mass would be constant for both spherical and irregular particles (which would not necessarily be the case if one compared only a linear diameter). Equal volumes and masses would therefore allow us to study deformation of the two different morphologies at a constant kinetic energy. The deformation occurs as this kinetic energy dissipates after the collisions. Therefore, equi-kinetic energy comparisons allow us to isolate the effect of morphology. Different scenarios of conical particles (which were chosen to approximate the irregular particles) are also chosen by choosing different apical angles which is commonly observed.

We have used a numerical model which is already tested and have been used by several authors before to determine the critical velocity which is our focus. The theory of adiabatic shear instability (ASI) is a well-known theory and several researchers have confirmed the theory. Thus, the model itself could give us better prediction of the critical velocities and the deformation behavior in comparison with the semi-empirical relations used in the papers cited above. Based on DE and porosity measured, the authors in the paper (Ref 7) suggested the spherical medium powder to have the best cold sprayability. On the other hand, we believe the scenario changes completely when volume and the apical angle of the irregular particles are also considered. For example, for equivalent volume of 8187 μm^3, spherical particle and conical particle with apical angle of 50° show similar critical velocity. We have been also able to show that, for similar particle volume with two different morphology, the deformation behavior of the conical particles with larger apical angle is very close to the spherical ones. One of the issues of irregular particles is suggested to be the lower flowability and hence suggested not to be good candidate for cold spraying. However, we believe that irregular particles with smaller volume (having flowability) with larger apical angle will be a good choice for cold spraying which will have lower critical velocity if compared to spherical particles with the same volume. Thus, the correct optimization of particle morphologies would benefit us with a higher deposition efficiency.

Both particle size and particle morphology seem to be important factors for coating deposition in a cold spraying process. A number of investigations are present in the literature that deals with the coating characteristics for both spherical and irregular particles. However, to the knowledge of the authors no report is available in the literature that deals with the systematic investigation on the effect of particle morphology on the critical velocity and deformation behavior in a cold spraying process. We address this deficiency in the literature by numerically investigating the deformation behavior of two different powder morphologies, i.e., spherical and conical. The near-surface regions of an irregular particle may be approximated by a combination of conical particles for modeling the edges and vertices in the irregular geometrical shapes—hence the choice

of particle morphologies in this paper. Moreover, the effect of particle shape and size on the critical velocity has been also analyzed. The present work is in that way a novel attempt to investigate the effect of particle size and morphology on the critical velocity and deformation behavior.

FE analysis of spherical and conical Cu particles with varying sizes, characterized by their volume, has been investigated. It has been demonstrated that the deformation characteristics and the critical velocity are a strong function of both the particle size and morphology. The paper has been structured as follows: Following an introduction to the problem and its definition in Sect. 1. Section 2 deals with the numerical modeling, methodology and computer simulation parameters implemented for the analysis. In Sect. 3, we present and discuss our results on the determination of the critical velocity, general deformation behavior and the coating characteristics. We finally draw our conclusions in Sect. 4.

2. Numerical Modeling

2.1 Methodology and Numerical Modeling

The finite element (FE) package ABAQUS has been used to perform nonlinear FE modeling of the high-velocity particle deformation during the impact with the substrate. Explicit time integration algorithm has been employed for the nonlinear analysis of deformation of the large particle. Due to the presence of geometrical symmetries, half of the particle and substrate have been considered. Hence, a 2D axisymmetric model has been used, as shown in Fig. 1(a) which also reduces the computational cost. The substrate has been considered as a cylinder with a radius and height of 10 times the particle radius which helps in avoiding the reflecting waves from the substrate bottom and far edges to reach the impact zone before the rebound of particle (Ref 27).

Dynamic temperature–displacement explicit analysis has been used which allows to study the impact due to the significant heating during an inelastic deformation of the material. In this model, particle and substrate interaction has been assumed to be an adiabatic process and hence temperature-dependent thermal conductivity and specific heat of the materials have been incorporated (Ref 28, 29). Surface-to-surface penalty contact algorithm and balanced contact pair formulation with penalty enforcement have been applied between the particle and the substrate which allows a small penetration between the particle and substrate. Four-node bilinear axisymmetric quadrilateral mesh elements with reduced integration and viscoplastic hourglass control (CAX4RT) have been used for the spherical particles. Mesh size of 0.5 μm has been used for both the particle and the $4R_p$ x $4R_p$ region of the substrate shown in Fig. 1(a), i.e., the region which experiences excessive deformation. For other regions of the substrate, a coarser mesh has been used. For conical particles, the axisymmetric geometry is considered as a triangular one and both the cases with the base of the cone and vertex of the cone hitting the substrate have been considered in our study. Figure 1(b-c) shows the arrangement of the impact for conical particles. ENCASTRE boundary condition has been applied at the bottom of the substrate which is considered fixed ($U1 = U2 = U3 = 0$) and a symmetry boundary condition about the X-plane ($U1 = UR2 = UR3 = 0$) has been applied along the Y-axis.

The Johnson–Cook plasticity model has been employed for describing the strain-rate and temperature dependence of material behavior during plastic deformation. The model is described as (Ref 30):

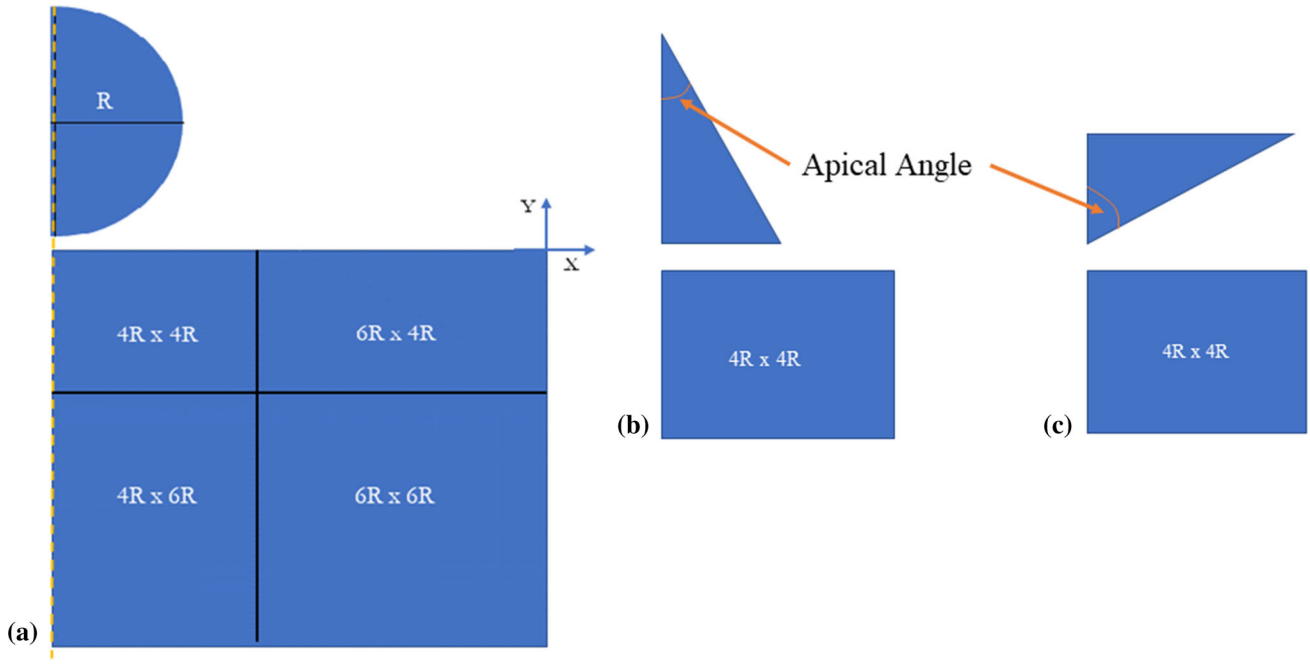

Fig. 1 Geometric model of the particle impact for the finite element analysis. (a) Spherical particle (case I), (b) basal contact for conical particle (case II) and (c) vertex contact for conical particle (case III). Only the second quadrant of the substrate which makes the first contact with the particle is shown for the conical particles

$$\sigma = \left(A + B\varepsilon^{n}\right)\left[1 + C\ln\left(\frac{\dot{\varepsilon}}{\dot{\varepsilon}_0}\right)\right]\left[1 - (T^{*})^{m}\right] \quad \text{(Eq 1)}$$

where σ is the equivalent flow stress, ε, $\dot{\varepsilon}$ and $\dot{\varepsilon}_0$ are the equivalent plastic strain, strain rate and normalizing reference strain rate. The constants A, B, C, n and m are the material constants. T^{*} is the normalized temperature, $T^{*} = \frac{T - T_r}{T_m - T_r}$, T_r is the reference transition temperature and T_m is the melting temperature. Considering the elastic response of the materials to follow linear elasticity model, Mie–Grüneisen equation of state has been used. The material properties used in the simulation are shown in Table 1.

2.2 Numerical Simulations

This work deals with the impact of high-velocity single copper particles on stainless steel 304L using numerical simulation. Both spherical and conical particles have been chosen with varying sizes. Comparing the particle size when morphologies are different presents a challenge. For example, a spherical particle is characterized by its radius, whereas a conical shape is characterized by its basal radius as well as the height. Hence, while measuring the size of different particle morphology, the characteristic dimensions are not consistent. Therefore, in this work, the dimensions of different shapes have been characterized by their volume and particles with identical volumes for different morphologies have been compared. Table 2 shows the dimensions of the geometry of the particles used in the simulations. The angle mentioned in the table is the angle between the hypotenuse and the height of the triangle which will be created for an axisymmetric conical case and we define this angle as the apical angle. For conical particles, we investigate both the cases of vertex and the basal impacts on the substrate.

The impact velocity of the particles has been varied from 100 to 600 m/s for each of the cases I-IV shown in Table 2 for both spherical and conical particles. It may be noted that the velocity shown in Table 2 refers to the velocity of the particle prior to impingement on to the substrate. This velocity is not same as the velocity of the particle emerging from De-Laval nozzle; hence, the effect of drag coefficient is neglected as a first approximation. The initial temperature of the particle as well as the substrate has been considered as 300 K. The value of 300K was chosen primarily due to two reasons

(a) Most studies in the literature (Ref 1, 3, 12, 27) assumed the temperature to be 300K. Therefore, for the sake of comparison of our work with the research previously reported, a value of 300 K was used.
(b) The simulation results will depend to an extent on the initial heating of the gas. However, the velocities are a function of temperature as well as pressure. Experimentally, a whole range of temperature and pressure combinations can be adopted. Without a priori information about the temperature that one would use, it was not possible for us to select a specific value and hence we decided upon using a value that has been commonly looked at in the literature.

All the impact conditions, i.e., initial temperature, mesh size, boundary conditions, etc., have been kept similar for both the cases to maintain consistency in our model. The initial distance between the particle and substrate has been kept 5 μm for all the simulations. Conical particles in axisymmetric case is considered to be a triangle. These conical particles can impinge upon the substrate with two distinct orientations while maintaining the axisymmetric conditions in the simulations, viz., collisions along the basal face and collisions with the vertex. We have studied the impact behavior for both the cases.

Table 1 Material properties used in the FE analysis

Properties with units	Copper	SS304L
Density, ρ, kg/m^3	8.9 x 10^3	7.92 x 10^3
Shear modulus, G, GPa	44.7	74
Thermal conductivity, λ, W/m·K	386.5	16.3
Specific heat, c J/kg ·K	383	499
Sound velocity, c_0, m/s	3940	4940
Slope in Us versus Up, s	1.489	1.49
Grüneisen coefficient, Γ_0	2.02	1.93
Yield stress, A, MPa	90	250
Hardening constant, B, MPa	292	480
Hardening exponent, n	0.31	0.35
Strain rate constant, C	0.025	0.03
Thermal softening exponent, m	1.09	1
Melting temperature, T_m, K	1356	1375
Reference temperature, T_0, K	298	298

3. Results and Discussion

We have investigated the effect of morphology and size on the deformation behavior of cold-sprayed powders. Two different particle morphologies, i.e., spherical and conical, have been considered for the numerical study. The geometry of the spherical particles is well defined and their size can be characterized by their radius. The cones, however, show greater diversity. The geometry of the cone can be manipulated by controlling the apical angle (as defined in Fig. 1). Similarly, the size of the cones can no longer be characterized by a single linear dimension. Hence, we have opted to characterize the size of cones by their volume. A change in particle volume (for a given particle velocity) affect the kinetic energy, which is dissipated as heat upon collision with the substrate and, in turn, influences the deformation behavior during the collisions. Hence, a comparison between the two morphologies is drawn only for equi-volume particles. Based on these considerations, the work presented in this paper is covered by three different cases, as defined below

Case I: Deposition of spherical particles

Case II: Basal contact with conical particles, where the basal region of the cone strikes the substrate.

Case III: Vertex contact with conical particles, where the vertex for which the apical angle was measured strikes the substrate.

For spherical particles, critical velocity depends on the particle size and decreases with an increase in particle size. A number of authors discussed this aspect in the literature (Ref 2, 3, 8). In addition, a comparative study has been made on the deformation behavior of the spherical particles and conical particles. For the conical particles, critical velocity decreases when the volume is kept constant and the apical angle is

Table 2 Dimension of the particles

Case	Particle type	Diameter, μm	Height, μm	Angle, degrees	Volume, μm^3
I	Spherical	5	…	…	66
		10	…	…	524
		25	…	…	8181
		55	…	…	87111
II	Conical (Basal impact)	6.61	5.723	30	65
		13.21	11.44	30	522
		33.04	28.62	30	8179
		72.69	62.96	30	87090
III	Conical (Vertex contact, varying volume)	8.4	28.62	10	529
		19.8	28.62	20	2937
		33.04	28.62	30	8179
		72.7	28.62	50	39600
		200	28.62	75	299699
	Conical (Vertex contact, constant volume)	28.4	38.7	20	8172
		33.04	28.62	30	8179
		42	17.7	50	8174

increased. However, an increase in critical velocity is observed for constant apical angle and increase in volume.

3.1 Critical Velocity

The particle size affects both, the critical velocity for adhesion and the deformation characteristics of the powder particle. We individually examine the role of particle size for all the three cases highlighted above.

3.1.1 Case I: Spherical Particles. This study deals with the critical velocity and deformation characteristics of the spherical particles in the size range of 5-55 μm (66-87111 μm^3) at different velocities. The critical velocity was found to decrease from 400 m/s for a particle size of 5 μm to 250 m/s for a particle size of 55 μm. The observed results are in accordance with experimental and numerical studies by other researchers (Ref 2, 7, 8, 21). The results are close to the critical values obtained experimentally which is in the range of 300-550 m/s for particle diameter 10-60 μm (Ref 17, 31, 32). The critical velocity was estimated by considering the variation in temperature and PEEQ values following the particle/substrate collisions. Figure 2(a-b) shows the plot of temperature and effective plastic strain, respectively, for the monitored element at different particle velocities for a spherical particle of 524 μm^3 (10 μm diameter). It is found that the effective plastic strain increases with an increase in the impact time of the particle. However, a sudden increase in plastic strain was observed beyond the impinging velocity of 375 m/s. The time–temperature plot at the same velocity also shows the similar jump in the temperature of the monitored element (Fig. 2). This increase in plastic strain and temperature is associated with the onset of adiabatic shear instability (ASI). This is a well-established phenomenon to describe the bonding mechanism in cold spraying process. This phenomenon ensures that the particle sticks to the substrate instead of recoiling. This velocity of adhesion is referred to critical velocity for a particular powder/substrate combination (Ref 1). It should be noted (Fig. 2) that for particle velocities 250 and 300 m/s, temperature increases on impact at time 27 and 24 ns, respectively, and then decreases. However, for 375 m/s, temperature increases on impact at around 15 ns, then there is again a

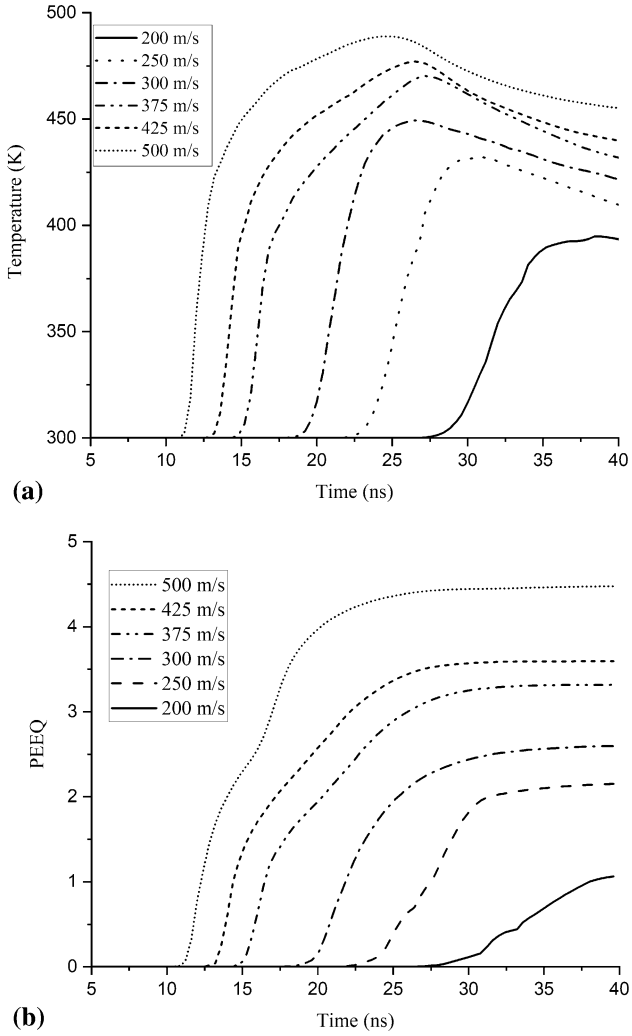

Fig. 2 Plot of change of temperature and effective plastic strain (PEEQ) with time for 10 μm diameter spherical particle

temperature rise for the second phase in time 15-25 ns and then it decreases. PEEQ on the other hand saturates after impact for velocities 250 and 300 m/s but for 375 m/s it starts saturating after the second sharp rise. The second phase is due the jetting at the interface between the particle and the substrate. This trend is observed for higher impact velocities too. And hence, the threshold velocity at which the jetting starts is considered as the critical velocity.

We have used the same model in our previous work on prediction of critical velocities of Cu, Ti, Ni and Al powders of particle size 25 μm and have shown a good agreement with experimental as well as theoretical predictions (Ref 3), and hence, we have a good reason to believe that the numerical model used is quite effective. Moreover, using 3D Lagrangian and Sobolov space Ghelichi et al. (Ref 33) found critical velocities for spherical particles in the range of 410-420 m/s for Cu using 3D numerical modeling. Yokoyama et al. (Ref 34) predicted a critical velocity of 210 m/s for Cu on Carbon steel using 2D axisymmetric model and extrapolating to zero mesh size. Adaptive mesh using CTH code predicted 570-580 m/s (Ref 35). Using shear localization parameter, critical velocity of 574 m/s for Cu particle of size 5-25 μm was determined. Using semi-empirical relations, Schmidt et al. (Ref 11) showed the critical velocity to be ranging from 462 to 617 m/s for Cu particle impacting on Cu substrate for particle size 5-25 μm. From direct experiments, Raletz et al. (Ref 32) found a critical velocity of 555 m/s particle size 10-33 μm. Therefore, there is a broad spectrum of critical velocities (approximately 210-620 m/s) obtained till now using different methodologies and our prediction does fall in this range. The spectrum of estimated value of critical velocity is wide for a particular material owing to the fact that a number of factors affect the estimation of critical velocity for a particular material, i.e., mesh size, mesh type, type of elements used for modeling, etc. Moreover, some physical parameters can also affect the calculation significantly such as surface roughness of the substrate and material properties.

3.1.2 Case II: Conical Particle, Basal Contact. Figure 3a-b shows the time evolution of temperature and equivalent plastic strain (PEEQ) with time for a conical particle of volume 520 μm^3 (CASE II). It may be noted that this conical particle we are considering is equivalent to a spherical particle with a 10 μm diameter in terms of volume. In this case, it is considered the base of the particle impacted with the substrate surface. This result is in contrast with the results found from the impact of the spherical particles with substrate (Case I). In this case, sudden jump in effective plastic strain (PEEQ) is absent. The increase in effective plastic strain monotonically increases with an increase in impingement velocity of particles. A similar observation has been made in the case of temperature as well. Both effective plastic strain and temperature saturate after a certain impact velocity. Similar evolution behavior is observed as we increased the volume of the conical particles from 65 to 87090 μm^3 (similar to the volume range for spherical particles considered in our study) (refer to Table 2). The variations in temperature at initial temperature are because of the non-uniform impact of the particle on the substrate and are shown later in the section #3.2, 'General Deformation Behavior.'

3.1.3 Case III: Conical Particle, Vertex Contact. The behavior is, however, different for the conical particles when the vertex of the particle impinges on the substrate (CASE III) in contrast to basal contact of the particle with the substrate

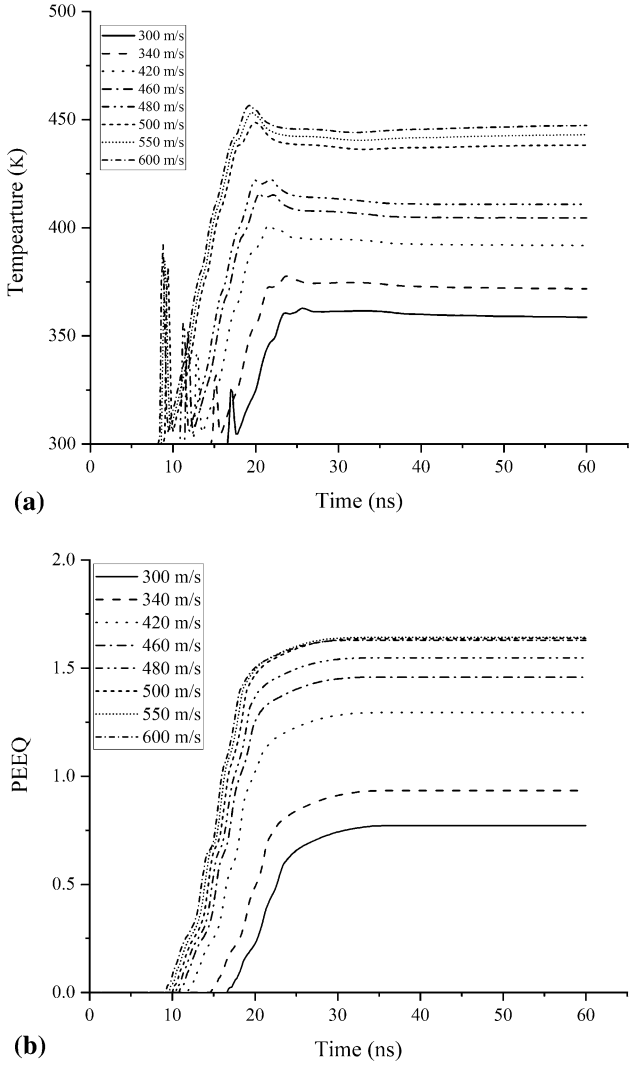

Fig. 3 Plot of temperature (a) and effective plastic strain (b) (right) for conical particles with base contact for a 10 μm equivalent of spherical particles with volume of approximately 520 μm^3

(case II, presented above). Figure 4a-b shows the temporal evolution of both temperature and equivalent plastic strain for a conical particle with volume of approximately 2987 μm^3 (Case III with apical angle of 20 degrees) for the case of vertex impingement of particle with the substrate. The variation of the temperature and PEEQ with time is similar to the spherical particles where, a sudden rise in both the quantities is visible although there is a minimal jump. After a threshold velocity (300 m/s), however, lip formation starts and the corner of the particles ejects out of the substrate at around 33 ns. This is the same time at which PEEQ rises sharply for particle velocity 300 m/s and hence is considered the critical velocity for the case. When we increase the volume of the particle to 8187 μm^3, keeping the angle fixed at 20 degrees, the critical velocity is observed to be increased to 400 m/s.

The temporal evolution of temperature and PEEQ is shown in Fig. 5 (a)-(b) for conical particle with an angle of 50 degrees (with a volume of 39600 μm^3). The sharp increase in both temperature and PEEQ is more prominent with the increase in apical angle. As the angle increases, the deformation of conical particles begins to resemble a sphere. This in itself is an

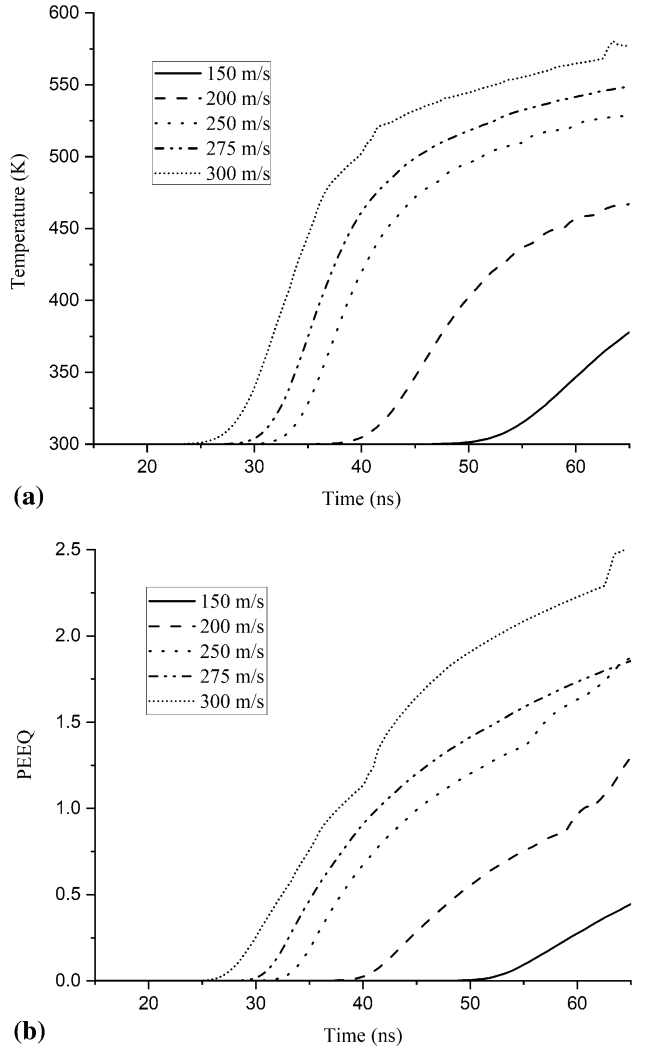

Fig. 4 Plot of temperature (a) and effective plastic strain (PEEQ) (b) for a conical particle with apical angle of 20 degrees and volume 2937 μm^3

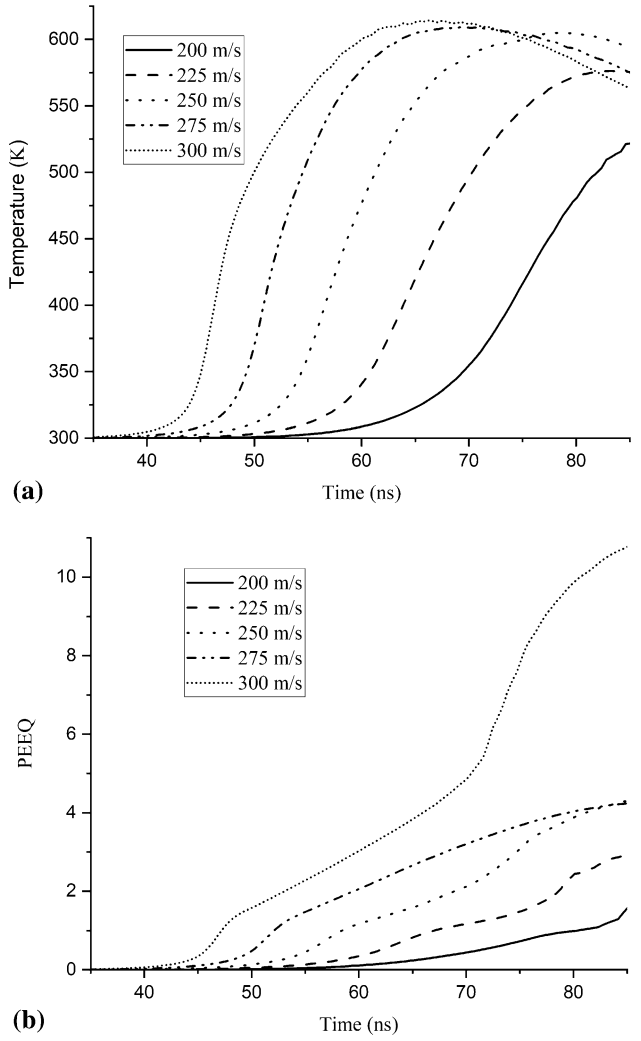

Fig. 5 Plot of temperature (a) and effective plastic strain (PEEQ) (b) for a conical particle (angle 50 degrees and volume 39600 μm^3) with vertex contact

expected result, since increase in apical angle effectively increases the curvature at the cone tip and makes the vicinity of contact more similar to a sphere. A critical velocity of 300 m/s is observed with a volume of 39600 μm^3. As we decrease the volume to 8189 μm^3, keeping the apical angle constant, the critical velocity decreases to 275 m/s. The conical particles, therefore, were observed to differ from the spherical particles with respect to the variation of critical velocity as a function of size. Therefore, critical velocity increases with an increase in volume for conical particles with the same angle. Instead, analogous to spherical particles, critical velocity decreases with increase in volume corresponding to increase in angle. The range of critical velocities for different scenarios from is Fig. 5 illustrated in Table 3.

To study the effect of morphology, we have analyzed the von Mises stress at different particle velocities (Fig. 6). Only Case I and Case III have been shown in this figure, since the critical velocity for case II could not be well-determined (due to the non-uniform impact), The trends observed for the 25 µm spherical particle are very similar to the 50° conical particle with apical collision, when the volume is same for both the particles (approximately 8179 μm^3). The stress of both particles increases gradually up to 275 m/s which is the observed critical velocity. At particle velocity 300 m/s, the stress values for both the particles are approximately same, although the conical particle started with lower stress values at lower velocities. Instead, the conical particles with 50° angle having much higher volume of 39,600 μm^3 have a very low stress values at lower particle velocities, increasing gradually until 275 m/s and then increases sharply and have higher stress values comparing to the conical particles having the same angle but lower volume. For conical particles with lower apical angles, for example with an apical angle of 20°, it is observed that at lower velocities (100-225 m/s), particle with larger volume has lower stress. At a higher velocity of about 300 m/s, stress of both the particles with different volume becomes similar. Hence, we see that at smaller apical angles, there is minimal effect of volume; however, as we increase the apical angle, the volume of the particles makes a difference. Smaller angles (for a fixed volume) imply sharper curvature and greater stress intensification. Therefore, the role of the angle is more critical. The critical velocities found for different cases are summarized in Table 4.

Table 3 Critical velocities obtained for different scenarios from Fig. 2, 3, 4 and 5

Figure no.	Morphology and volume of particle in μm^3	Critical velocity in m/s
2	Spherical, 524	350
3	Conical base, 520	Impact is non-uniform and hence critical velocity could not be found
4	Conical impact (20 degrees, 2987)	300
5	Conical impact (50 degrees, 39600)	300

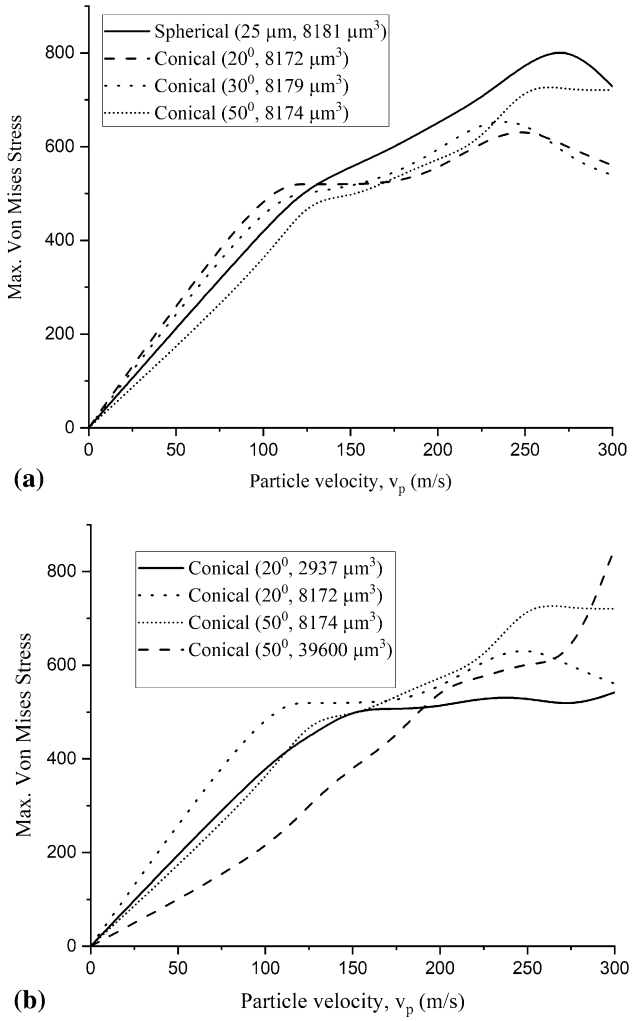

Fig. 6 Variation of maximum von Mises stress with particle velocity: (a) Spherical and conical with same volume and (b) conical with varying volumes

3.2 General Deformation Behavior

Figure 7 (top panels) shows the deformation behavior of 25 μm spherical particle at 300 m/s at time 18, 22 and 36 ns. The spherical particle deforms adopting an ellipsoidal shape. Intensive deformation at about 36 ns leads to the jet formation due to the ASI which was briefly discussed in the previous section. This phenomenon ultimately leads to a sharp increase in temperature and effective plastic strain (PEEQ). The spherical particle shows radial symmetry during the deformation process and the contact area increases uniformly. The conical particle, however, shows a marked difference in deformation characteristics. In case II (base impact of the conical particles), the basal vertex of the cone shows a much higher degree of deformation. This is the first region that comes in contact with the substrate and deforms significantly during basal impact of the conical particle. The vertices of a cone are expected to be regions of higher stress concentration when compared to the basal regions. Therefore, one expects that the Tresca yield criterion to be satisfied near the vertex region, experiencing force much more rapidly than the base. Subsequently, with increasing contact time, the remaining basal surface deforms as well. Thus, the contact area is never uniform for conical particles. Interestingly in case III, for the particle with 30^0 apical angle (shown in Fig. 7 (bottom panels)), there is no deformational change in the substrate and the particle do not impinge into the substrate at all. Rather, the deformation occurs at the vertex of the conical particle undergoing collision leading to a large compression and flattening. A similar behavior is observed for vertex impact of conical particles with an apical angle of 10° and 20°. The behavior of the particles, however, changes when the apical angle of the conical particles increases. The particles exhibit an extensive deformation at the vertex region upon impingement on to the substrate (shown in Fig. 8 for apical angle of 75 degrees). The deformation looks very similar to the spherical particles. The deformation of the substrate is more severe for the spherical particles.

The extent of deformation is primarily measured by the estimation of compression ratio and flattening ratio. For spherical particles and conical particles with vertex contact, these indices are estimated and discussed next. For conical particles with basal contact, the temperature, and equivalent plastic strain saturates at critical velocity. Hence, no marked changes are observed in the deformation of the particles with velocities higher than the critical velocity. Therefore, estimation of deformation indices, i.e., compression ratio and flattening ratio, is not possible.

3.2.1 Flattening Ratio. The flattening ratio (F) is defined as the ratio of the spreading diameter of the flattened particles (D) and the original diameter of the particle (d_p). Here, spreading diameter is the diameter of the particle on maximum deformation, perpendicular to the direction of the impact.

$$F = D/d_p, \qquad \text{(Eq 2)}$$

For a given particle size, the flattening ratio first increases gradually and then there is a steep increase as we move to higher velocities (Fig. 9). This steep increase is found to be higher for conical particles as compared to the spherical particles. For spherical particles, the flattening ratio also decreases with an increase in particle size from 5 to 25 μm, i.e., that is increase in volume. Similar behavior is also observed for conical particles, where, as we keep increasing the volume of the particles, keeping the height of the particles same (Case III), flattening ratio decreases. The strength of the flattening is much higher for the conical particles as compared

Table 4 Critical velocities obtained from numerical experiments

Case	I				III		III		
Particle Morphology ad size	Spherical (Diameter in μm)				Conical Vertex Impact (Increase in volume for a constant angle 50°) (Volume in μm^3)		Conical Vertex Impact (Increase in angle for a constant volume ~ 8187 μm^3) (Angle in degrees)		
	5	10	25	55	8174	39600	20	30	50
Critical velocities in m/s	400	375	275	250	275	300	400	325	275

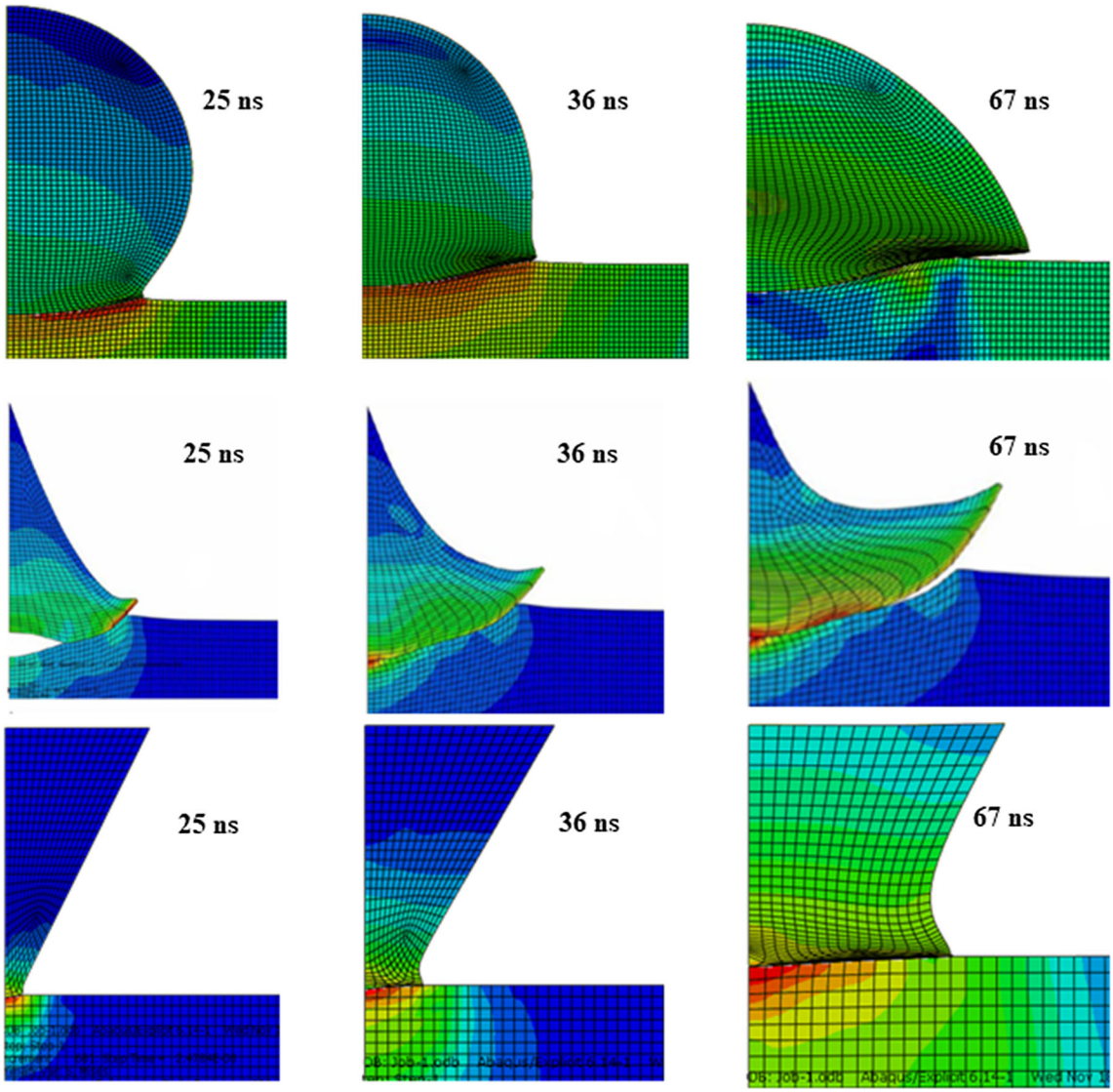

Fig. 7 Deformation behavior of spherical particles (top), conical particles with base impact (center) and conical particles with vertex impact (bottom) particles at the time of impact (left), intermediate (center) and maximum deformation (right) at particle velocity of 300 m/s

to spherical particles. Similarly, even if we keep the volume constant and increase the angle of the conical particles (i.e., start approaching shallower curvatures), flattening ratio decreases. Interestingly though, the flattening ratio does seem to be dependent on the volume of the particle. If we compare particle with 20° apical angle and a volume of 2937 and 8179 μm^3, respectively, then the flattening ratio is found to be lower for particle with higher volume. This is in line with our

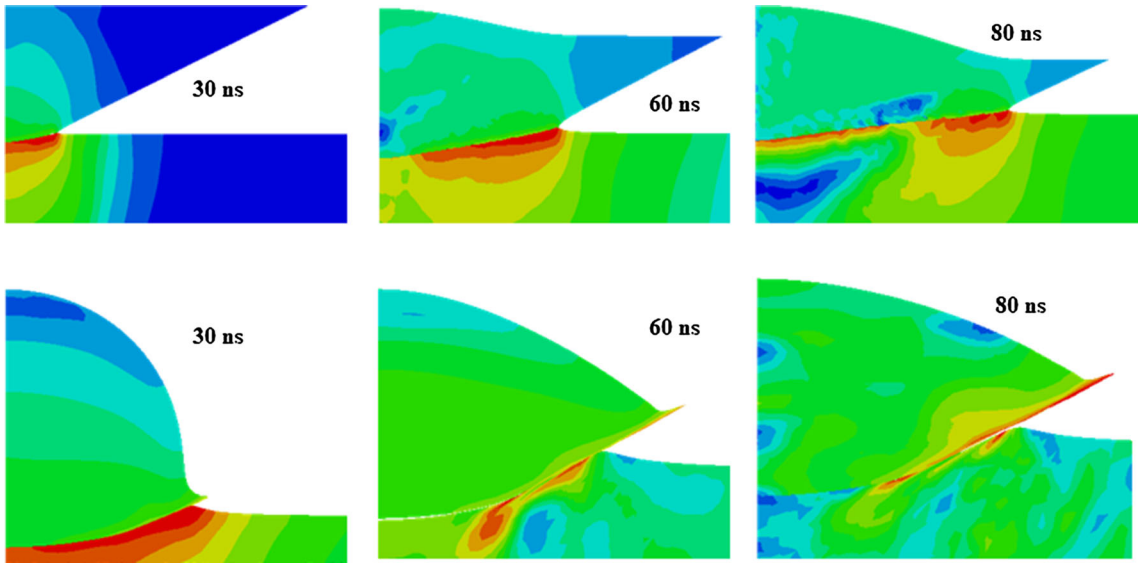

Fig. 8 Deformation behavior of conical particles with 75 degrees angle with vertex impact (top frames) at 300 m/s and 25 μm spherical particles at particle velocity of 400 m/s

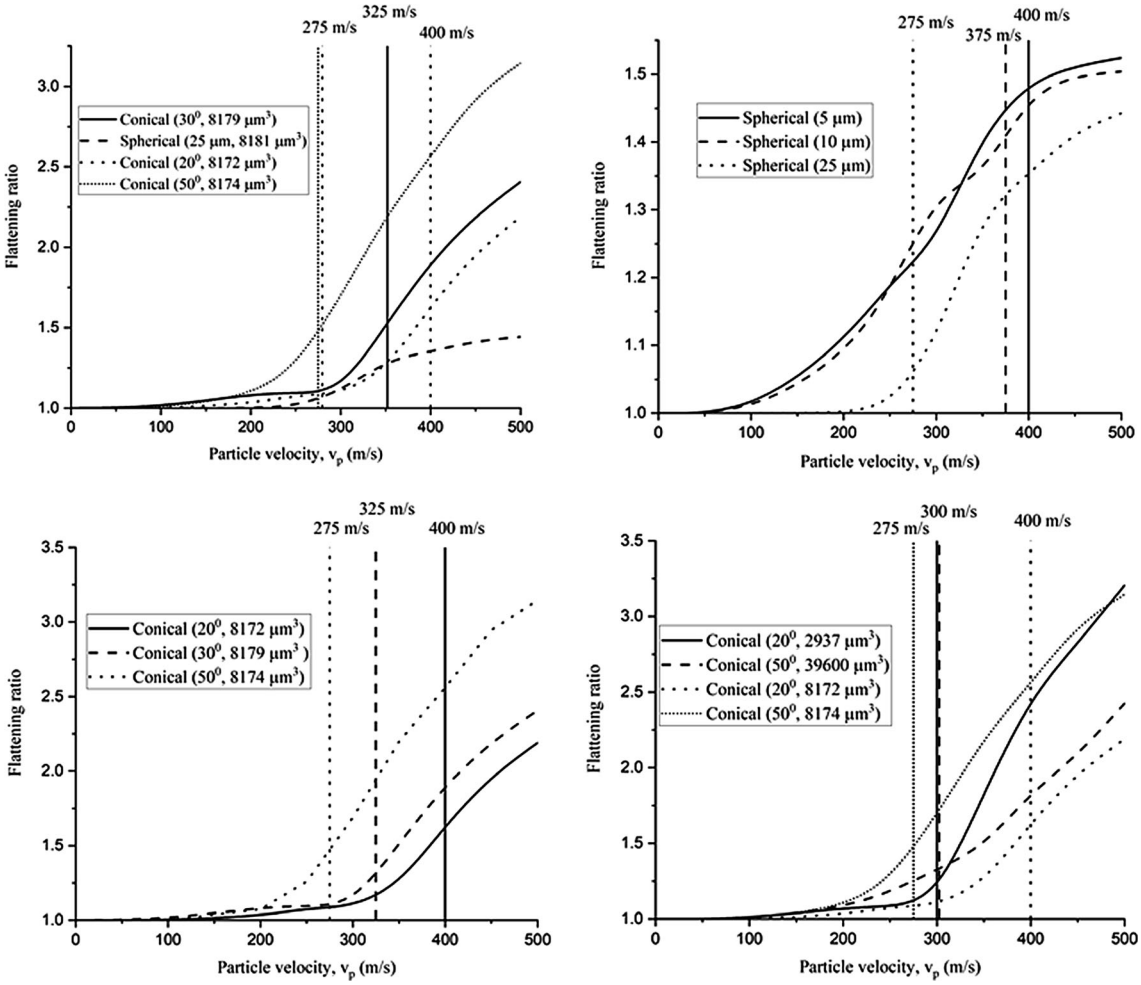

Fig. 9 Flattening ratio of different particle morphologies. Vertical lines represent the critical velocity measured corresponding to each of the cases studied

observations in Fig. 6, where the smaller particle shows a higher von Mises stress. Similar observations can be made for particle with 50^0 apical angle but with different volumes.

3.2.2 Compression Ratio. The compression ratio is defined as

$$C = (h_p - H)/\, h_p \qquad \text{(Eq 2)}$$

where h_p is the original height of the particle and H is the height of the flattened particle in the direction of impact in the direction of impact. Compression ratio also increases with an increase in the particle velocity of impingement. This is due to the fact that plastic deformation is more severe with an increase in the kinetic energy of the impinging particle prior to impact. Similar results are also observed in the case of conical particles, where compression ratio decreases with an increase in the apex angle of the particles.

The critical velocities for each of the cases are represented by vertical lines in Fig. 9 and 10. The steep increase in both the flattening ratio and the compression ratio is noticed once the particle velocity is beyond the critical velocity. A summary of the deformation behavior is presented in Table 5.

We numerically investigated the effect of particle size and morphology on the deformation characteristics and critical velocity during a cold spray process for Cu particles on a steel substrate. It is observed that an increase in the size of spherical particles results in a reduction in critical velocity, an increase in von Mises stress at a given velocity. Moreover, a reduction in both flattening and compression ratios is found with an increase in the size of the spherical particles. These results are in agreement with the results reported in the literature (Ref 7). When we consider different powder morphologies (conical particles) multiple situations arise. When the contact is along the base of the conical shapes, it is seen that the particle corners deform rapidly even as there is a separation of the particle surface from the surface, which in general would indicate poor deposition. When the particle–substrate collisions occur at the vertex of the cone, it is observed that an increase in the apical angle, for a constant volume, results in reduced critical velocity, increased von Mises stresses and enhanced flattening and compression ratios. Unlike the spherical particles, vertex impact for conical particles results in greater deformation in the particle as compared to the substrate. The presence of sharp curvature at the vertex of a cone results in a region of high stress concentration within the particle, thereby introducing a much greater deformation in the particle as opposed to the substrate.

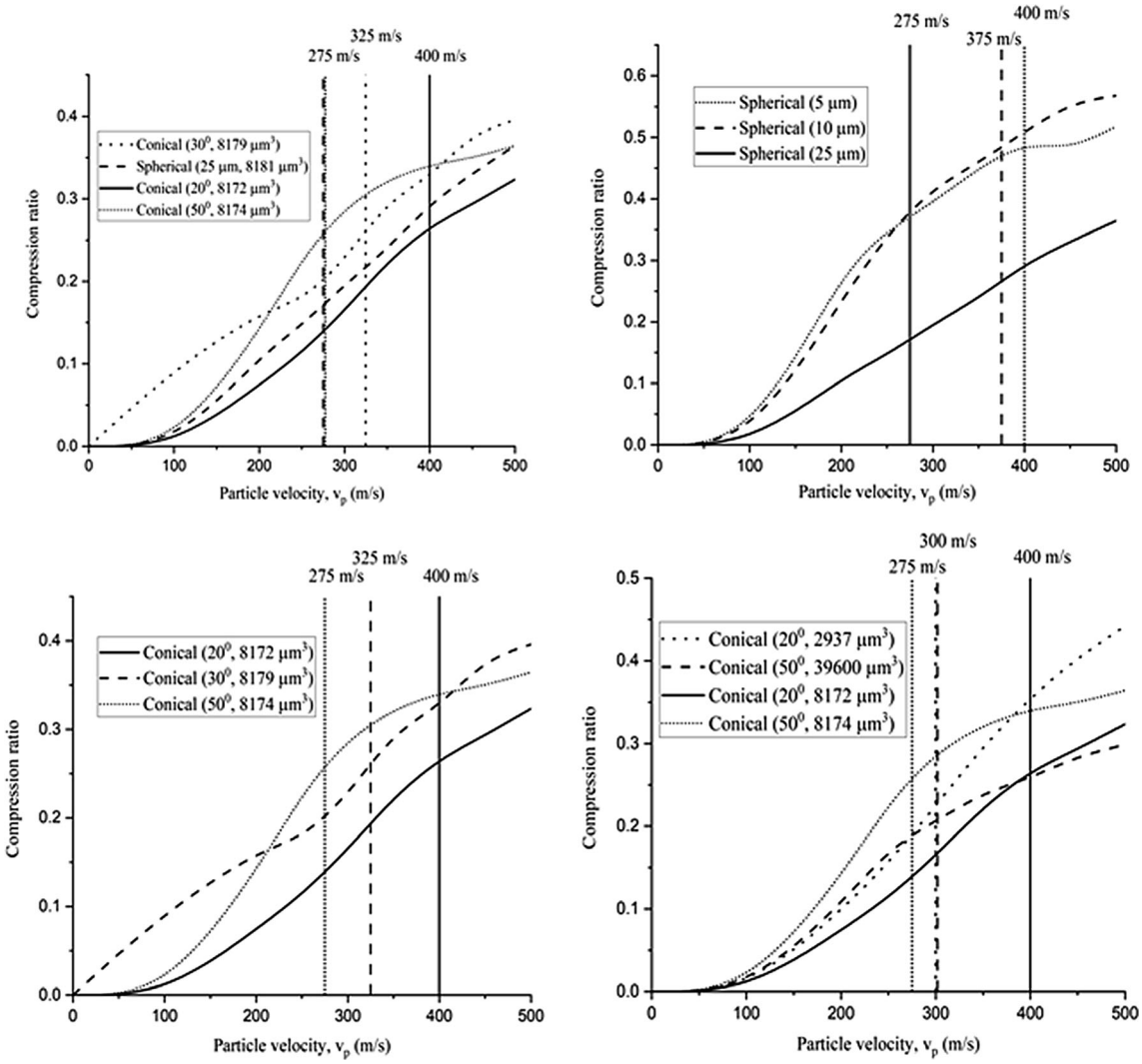

Fig. 10 Compression ratio of the particles. Vertical lines represent the critical velocity measured corresponding to each of the cases studied

Table 5 Summary and comparison of deformation characteristics of the various morphologies considered in the study

Size and morphology	Volume	Angle	Critical velocity	Max. von Mises Stress	Flattening ratio	Compression ratio
Spherical (Case I)	↑	…	↓	↑	↓	↓
Conical (Vertex contact)	Constant (∼ 8174 μm^3)	↑	↓	↑	↑	↑
Conical (Vertex Contact)	↑	Constant (50°)	↑	↑	↓	↓

As the angle is increased keeping the volume constant, the height of the cone reduces. Consequently, the compression ratio (as defined in eq. 3) also increases, since the height of the cone appears in the denominator. On the other hand, a near opposite behavior is observed when the apical angle is held constant and the volume of the cone is increased. Increase in volume results in an increase in the particle velocity, which is opposite to the trends observed for spherical particles. The von Mises stress also increases for a given particle velocity (which is similar to the behavior of spherical particles, as well as similar to the trends in variation of von Mises stress at constant volume and increasing apical angle). The variation in compression ratio and flattening ratio with the increase in volume is similar to the results observed for spherical particles.

4. Conclusion

This work deals with the estimation of critical velocity and deformation behavior of the powder particles with the different powder particle morphologies and sizes. Several reports available in the literature on the deposition mechanism of cold spraying process considers spherical particle morphology of the powders. Spherical particles will result in greater uniformity of results. However, while preferred, not all powders have a spherical morphology. Therefore, it is important to understand the effect of non-spherical shapes (modeled here as conical) on the deposition/deformation characteristics. Essentially, having performed the simulations over a range of apical angles, we estimate an envelope of deposition characteristics as particles change their shape from sharp cones (small apex angle) to blunt cones (larger angles) where the behavior starts resembling that of the spherical particles. To this extent, the work provides a measure of the scatter that can occur in experiments as often an assortment of shapes is present in the powder blends.

The variation in the size and morphology of particles results in a change in the curvature (and hence stress concentration) as well as the kinetic energy (at a given velocity). When the curvatures are sharp (sharper angles in the conical particles, or very small volumes of the conical particles), the extent of stress concentration is high. This, in turn, leads to preferential deformation of the particle, which does not necessarily result in a corresponding substrate deformation, and thus may not result in better deposition of the coating. However, as the curvature reduces (increased angle for a given volume), a greater deformation of the substrate takes place with increased contact area with the substrate, which in turn results in better adhesion. This is also manifested in enhanced flattening and compression ratios. For a given apical angle, however, an increase in volume results in a behavior similar to spherical particles in terms of flattening and compression ratios, i.e., they decrease with increased particle sizes.

Irregular particles are shown to have higher deposition efficiency in comparison with spherical particles. At the same time adhesion of irregular particles is shown to be poor because of lower deformation. We have shown that the deformation behavior of the conical and spherical particles is similar when the apical angel is large. It is also important to mention that the velocity at which the deformation of conical particles is similar to the spherical particles is less than the velocity at which the spherical particles are deformed. Therefore, although gas-atomized spherical particles are easily available, however, we believe, calibrated irregular particles can result in a higher deposition efficiency and adhesion at lower particle velocity as compared to the spherical particles.

Acknowledgments

This work is financially supported by the Faculty Research and Innovation Award (FRIA) grant and the authors Dr. Lopamudra Palodhi and Dr. Harpreet Singh are grateful to Indian Institute of Technology Ropar, Rupnagar (India).

References

1. H. Assadi, F. Gärtner, T. Stoltenhoff and H. Kreye, Bonding mechanism in cold gas spraying, *Acta Mater.*, 2003, **51**, p 4379–4394.
2. M. Hassani-Gangaraj, D. Veysset, K.A. Nelson and C.A. Schuh, In-situ observations of single micro-particle impact bonding, *Scripta Mater.*, 2018, **145**, p 9–13.
3. L. Palodhi and H. Singh, On the dependence of critical velocity on the material properties during cold spray process, *J. Therm. Spray Tech.*, 2020, **29**, p 1863–1875. https://doi.org/10.1007/s11666-020-01105-7
4. T.H. Van Steenkiste, J.R. Smith, R.E. Teets, J.J. Moleski, D.W. Gorkiewicz, R.P. Tison, D.R. Marantz, K.A. Kowalsky, W.L. Riggs II. and P.H. Zajchowski, Kinetic spray coatings, *Surf. Coat. Technol.*, 1999, **111**, p 62–71.
5. T. Stoltenhoff, H. Kreye and H.J. Richter, An analysis of the cold spray process and its coatings, *J. Therm. Spray Technol.*, 2002, **11**, p 542–550.
6. H. Assadi, T. Schmidt, H. Richter, J.-O. Kliemann, K. Binder, F. Gärtner, T. Klassen and H. Kreye, On parameter selection in cold spraying, *J. Therm. Spray Technol.*, 2011, **20**, p 1161–1176.
7. W. Wong, P. Vo, E. Irissou, A.N. Ryabinin, J.-G. Legoux and S. Yue, Effect of particle morphology and size distribution on cold-sprayed pure titanium coatings, *J. Therm. Spray Technol.*, 2013, **22**, p 1140–1153.
8. T. Schmidt, F. Gärtner, H. Assadi and H. Kreye, Development of a generalized parameter window for cold spray deposition, *Acta Mater.*, 2006, **54**, p 729–742.
9. D.L. Gilmore, R.C. Dykhuizen, R.A. Neiser, M.F. Smith and T.J. Roemer, Particle velocity and deposition efficiency in the cold spray process, *J. Therm. Spray Technol.*, 1999, **8**, p 576–582.

10. C.-J. Li and W.-Y. Li, Deposition characteristics of titanium coating in cold spraying, *Surf. Coat. Technol.*, 2003, **167**, p 278–283.
11. T. Schmidt, H. Assadi, F. Gärtner, H. Richter, T. Stoltenhoff, H. Kreye and T. Klassen, From particle acceleration to impact and bonding in cold spraying, *J. Therm. Spray Technol.*, 2009, **18**, p 794–794.
12. G. Bae, Y. Xiong, S. Kumar, K. Kang and C. Lee, General aspects of interface bonding in kinetic sprayed coatings, *Acta Mater.*, 2008, **56**, p 4858–4868.
13. A. Manap, O. Nooririnah, H. Misran, T. Okabe and K. Ogawa, Experimental and SPH study of cold spray impact between similar and dissimilar metals, *Surf. Eng.*, 2014, **30**, p 335–341.
14. F. Meng, S. Yue and J. Song, Quantitative prediction of critical velocity and deposition efficiency in cold-spray: a finite-element study, *Scripta Mater.*, 2015, **107**, p 83–87.
15. S. Rahmati and B. Jodoin, Physically based finite element modeling method to predict metallic bonding in cold spray, *J. Therm. Spray Technol.*, 2020, **29**, p 1–19.
16. T.H. Van Steenkiste, J.R. Smith and R.E. Teets, Aluminum coatings via kinetic spray with relatively large powder particles, *Surf. Coat. Technol.*, 2002, **154**, p 237–252.
17. F. Gärtner, T. Stoltenhoff, T. Schmidt and H. Kreye, The cold spray process and its potential for industrial applications, *J. Therm. Spray Technol.*, 2006, **15**, p 223–232.
18. X.-J. Ning, J.-H. Jang and H.-J. Kim, The effects of powder properties on in-flight particle velocity and deposition process during low pressure cold spray process, *Appl. Surf. Sci.*, 2007, **253**, p 7449–7455.
19. G. Mauer, R. Singh, K.-H. Rauwald, S. Schrüfer, S. Wilson and R. Vaßen, Diagnostics of cold-sprayed particle velocities approaching critical deposition conditions, *J. Therm. Spray Technol.*, 2017, **26**, p 1423–1433.
20. C.-J. Li, W.-Y. Li and H. Liao, Examination of the critical velocity for deposition of particles in cold spraying, *J. Therm. Spray Technol.*, 2006, **15**, p 212–222.
21. P.C. King and M. Jahedi, Relationship between particle size and deformation in the cold spray process, *Appl. Surf. Sci.*, 2010, **256**, p 1735–1738.
22. B. Jodoin, L. Ajdelsztajn, E. Sansoucy, A. Zúñiga, P. Richer and E.J. Lavernia, Effect of particle size, morphology, and hardness on cold gas dynamic sprayed aluminum alloy coatings, *Surf. Coat. Technol.*, 2006, **201**, p 3422–3429.
23. N. Cinca, M. Barbosa, S. Dosta and J.M. Guilemany, Study of Ti deposition onto Al alloy by cold gas spraying, *Surf. Coat. Technol.*, 2010, **205**, p 1096–1102.
24. T. Marrocco, D.G. McCartney, P.H. Shipway and A.J. Sturgeon, Production of titanium deposits by cold-gas dynamic spray: numerical modeling and experimental characterization, *J. Therm. Spray Technol.*, 2006, **15**, p 263–272.
25. W. Wong, A. Rezaeian, E. Irissou, J.G. Legoux and S. Yue, Cold spray characteristics of commercially pure Ti and Ti-6Al-4V, *Adv. Mater. Res.*, 2010, **89**, p 639–644.
26. S.H. Zahiri, C.I. Antonio and M. Jahedi, Elimination of porosity in directly fabricated titanium via cold gas dynamic spraying, *J. Mater. Process. Technol.*, 2009, **209**, p 922–929.
27. J. Xie, D. Nélias, W.-L. Berre, K. Ogawa and Y. Ichikawa, Simulation of the cold spray particle deposition process, *J. Tribol.*, 2015, **137**, p 4.
28. C.Y. Ho, T.K. Chu, Electrical resistivity and thermal conductivity of nine selected AISI stainless steels, Thermophysical and Electronic Properties Information Analysis Center …, 1977
29. C.S. Kim, Thermophysical properties of stainless steels, Argonne National Lab., Ill.(USA), 1975
30. G.R. Johnson, W.H. Cook, Proceedings of the 7th International Symposium on Ballistics, The Hague, Netherlands, 1983, (1983)
31. C.-J. Li, H.-T. Wang, Q. Zhang, G.-J. Yang, W.-Y. Li and H.L. Liao, Influence of spray materials and their surface oxidation on the critical velocity in cold spraying, *J. Therm. Spray Tech.*, 2010, **19**, p 95–101. https://doi.org/10.1007/s11666-009-9427-x
32. F. Raletz, M. Vardelle and G. Ezo'o, Critical particle velocity under cold spray conditions, *Surf. Coat. Technol.*, 2006, **201**, p 1942–1947.
33. R. Ghelichi, S. Bagherifard, M. Guagliano and M. Verani, Numerical simulation of cold spray coating, *Surf. Coat. Technol.*, 2011, **205**, p 5294–5301.
34. K. Yokoyama, M. Watanabe, S. Kuroda, Y. Gotoh, T. Schmidt and F. Gärtner, Simulation of solid particle impact behavior for spray processes, *Mater. Trans.*, 2006, **47**, p 1697–1702.
35. M. Grujicic, C.L. Zhao, C. Tong, W.S. DeRosset and D. Helfritch, Analysis of the impact velocity of powder particles in the cold-gas dynamic-spray process, *Mater. Sci. Eng., A*, 2004, **368**, p 222–230.